Linearized Price-Responsive HVAC Controller for Optimal Scheduling of Smart Building Loads

Mohammad Ostadijafari, *Student, IEEE*, Anamika Dubey, *Member, IEEE*, and Nanpeng Yu, *Member, IEEE*

Abstract—The need to optimize the energy consumption of commercial buildings– responsible for over 40% of US energy consumption–has recently gained significant attention due to the call for energy efficiency. Moreover, the ability to participate in the retail electricity markets through proactive demand-side participation has recently led to the development of an economic model predictive control (EMPC) for these buildings' Heating, Ventilation, and Air Conditioning (HVAC) systems. The objective of this paper is to develop a price-responsive operational model for buildings' HVAC systems while considering inflexible loads and other distributed energy resources (DERs), including photo-voltaic (PV) generation and battery storage systems. A Nonlinear Economic Model Predictive Controller (NL-EMPC) is presented to minimize the net cost of energy usage by the buildings' flexible loads i.e. HVAC systems while satisfying the comfort-level of buildings' occupants. To improve the computational efficiency of the HVAC system controller, we propose a linearized economic model predictive controller (L-EMPC). The L-EMPC is a novel approximate linearized model for the NL-EMPC and is based on the feedback linearization technique. The proposed approach results in a controller for the building with the reduced complexity that accurately approximates the original nonlinear plant dynamics with its economic constraints. The efficiency of the proposed EMPC controllers are evaluated using several simulation case studies.

Index Terms—Economic model predictive control, Building thermal model, HVAC, Demand response, Feedback linearization.

I. INTRODUCTION

THE Heating, Ventilation, and Air Conditioning (HVAC) system is responsible for a significant proportion of the buildings' total energy consumption [1]. Recently, as a result of wholesale electricity market restructuring and development of retail electricity markets, researchers have explored the potential of commercial buildings in proactive demand-side participation. For example, in [2], authors proposed an MPC-based optimization approach to generate proactive demand-bid curves for the buildings to optimally schedule their energy consumption in response to the variable electricity prices. The optimization of buildings' energy consumption while satisfying the occupants' comfort requirements needs a price-responsive model for building thermal loads and advanced control methods for the HVAC systems [3]. In literature,

model predictive control (MPC) for both tracking a desired set-point and for economic optimization (using economic model predictive control/EMPC) has been employed to solve this problem [4].

MPC is a model-based controller that requires the dynamical model of the system to obtain optimal control inputs. The required model of the system must be sufficiently accurate to acquire a valid prediction of system states in a computation-ally tractable manner [5]. Building thermal model dynamics results in a nonlinear HVAC system model [2]. Recently, due to the computational complexity of nonlinear MPC, linear HVAC controllers designed with Jacobian-based linearization of building thermal dynamics have drawn significant attention. For example, in [6], [7], a Jacobian linearization approach is used to eliminate the system nonlinearity, and the resulting linear model is used to design a traditional MPC for temperature set-point tracking. In [8], authors use a feedback linearization approach to linearize the simplified nonlinear system model and develop a MPC technique to track set-point temperature using water-to-air heat exchange in HVAC systems. Similarly, assuming that the room temperature can vary in a short range, [9] and [10] propose a MPC-based control algorithm based on Jacobian linearization to co-schedule the HVAC system and battery storage units to reduce energy cost while meeting the HVAC system requirements.

Unfortunately, the Jacobian linearization approach is not valid when the desired room temperature obtained from the optimization problem varies significantly at different time-steps [11]. This is usually the case when the building is not occupied at certain times of the day and can be overheated or overcooled to achieve the desired economic objective. This case is of significant interest when optimizing the transacted cost of energy by leveraging the occupancy information of the building. Since the primary energy consumption for a building is due to its HVAC system, significant cost savings can be achieved using a price-responsive HVAC model that optimally schedules heating/cooling while taking the build-ing's occupancy information into account, as demonstrated using a nonlinear MPC-based optimization problem in [2]. Specifically, authors in [2] formulate a nonlinear MPC-based optimization problem in which, based on a bilinear model, the controller minimizes the cost of transacted energy while meeting the HVAC system's requirements and satisfying the comfort level of the occupants. Similarly, by proposing a nonlinear model for the overall cooling system, [12] presents a MPC scheme for minimizing the energy consumption.

A nonlinear MPC control (based on the nonlinear building thermal model dynamics) is time-consuming and may not be

practical for real-time control, especially when co-scheduling a large-number of buildings' flexible resources with time-varying price signals [3]. This calls for linearization methods that, unlike Jacobian-based methods, can accurately model the time-varying temperature set-points for HVAC systems while also co-scheduling all available buildings' flexible resources. To address this concern, in this paper we propose an approximate linearized economic model predictive controller (L-EMPC) for the buildings' HVAC systems while considering inflexible loads and other distributed energy resources (DERs) including photovoltaic (PV) generation and battery storage system. The performance of the proposed linearized controller (L-EMPC) is thoroughly validated against the original nonlinear MPC (NL-EMPC) using multiple case studies. The major contributions of this paper are listed below:

- We propose a novel L-EMPC controller for the buildings' HVAC systems. The proposed L-EMPC is based on a feedback linearization technique that, unlike Jacobian linearization, linearizes the nonlinear building thermal dynamical model without making any assumption regarding the allowable variations in a building's temperature set-points. The proposed L-EMPC model approximates the price responsive behavior of the original non-linear (bilinear) building thermal model while drastically reducing the associated computational cost.
- We describe the L-EMPC model for a home energy management system (HEMS) that includes models for the HVAC system, local DERs including PV and the battery energy storage, and controllers therein. We also include a detailed model for the battery energy storage system and demonstrate the effects of battery depreciation cost on the optimal control trajectory for the HVAC system and battery storage system.
- We present a thorough validation of the proposed L-EMPC model by demonstrating its: (1) accuracy in estimating original non-linear plant dynamics; (2) price responsiveness when subjected to uncertainty; and (3) price responsiveness when including local DERs (PV and battery storage). The results are benchmarked against the equivalent NL-EMPC HVAC controller. We demonstrate that the proposed L-EMPC model closely approximates the optimal control trajectory obtained for the equivalent NL-EMPC model.
- The bilinear model for a building thermal dynamics is compared against an equivalent Jacobian-linearized building thermal model. It is demonstrated that the Jacobian-linearized model cannot appropriately represent the building thermal dynamics when indoor temperature varies over a wider range and leads to undesirable control actions that violate designated occupants' comfort levels.

The rest of the paper is organized as follows: Section II describes the required component models that are used in the problem formulation. Section III provides the mathematical formulation for the proposed NL-EMPC and L-EMPC models and details different methods employed for eliminating the model nonlinearities. Section IV thoroughly validates the proposed controllers for varying system conditions and highlights the benefits of the proposed L-EMPC approach. Finally, Section V presents concluding remarks.

II. OVERVIEW OF THE PROPOSED FRAMEWORK

This section details mathematical models for a dynamical model for the building thermal load, battery energy storage systems, and photovoltaic (PV) generation panels.

A. Dynamical Model for Building Thermal Load

An accurate thermal model of a building can be obtained using building energy performance simulation (BEPS) tools such as EnergyPlus, TRNSYS, ESP-r [5]. Although these tools provide a building thermal model of high precision, mathematical descriptions of such models are incredibly complex which makes them intractable to use for online optimizations [13]. As a result, models with lower computational complexity are commonly used in the recent literature especially when implementing advanced model-based control methods such as MPC. For the building thermal load, the RC network model based on the analogy between the diffusion of heat and electrical charge, is commonly employed by the HVAC system engineering community [14]–[16]. This representation provides a useful tool for conceptualizing and quantifying the heat transfer problem. Here, we describe a bilinear model for the building thermal dynamics derived from the RC network model.

In general, if there are in total n nodes, m of which denote rooms, then $n - m$ remaining nodes denote walls. Using the same equations as detailed in [17], to describe rooms' and walls' temperatures for the sampling time K denoted by $\boldsymbol{T}_r^K$ and $\boldsymbol{T}_w^K$, respectively, and after zero-hold discretization [2], we obtain the following state-space equations representing the building thermal model that is bilinear in output and control decisions:

$$\boldsymbol{x}^{k+1} = \boldsymbol{A}\boldsymbol{x}^k + \boldsymbol{B}\boldsymbol{u}^k \circ (\boldsymbol{T_s} - \boldsymbol{y}^k) + \boldsymbol{E}\boldsymbol{d}^k \quad (1)$$

$$\boldsymbol{y}^k = \boldsymbol{C}\boldsymbol{x}^k \quad (2)$$

where, superscript k shows the sampling time and $\circ$ is the element-wise product operator for two vectors; $\boldsymbol{d}^k \in \mathbb{R}^l$ is the vector of environmental disturbance (with l number of the disturbance elements such as external temperature, solar radiation and internal gains, etc.); $\boldsymbol{A} \in \mathbb{R}^{n \times n}$, $\boldsymbol{B} \in \mathbb{R}^{n \times m}$, $\boldsymbol{C} \in \mathbb{R}^{m \times n}$ and $\boldsymbol{E} \in \mathbb{R}^{n \times l}$ are matrices obtained from a building thermal model representing time-invariant building parameters (see [6], [17] for more details); $\boldsymbol{x}^k = \begin{bmatrix} \boldsymbol{T}_w^k \\ \boldsymbol{T}_r^k \end{bmatrix} \in \mathbb{R}^n$ is the state vector representing the temperature of the network nodes; $\boldsymbol{u}^k \in \mathbb{R}^m$ is the vector of input variables whose elements (u_i^k) are air mass flow into each thermal zone; $\boldsymbol{y}^k = \boldsymbol{T}_r^k \in \mathbb{R}^m$ is the output vector of the system; and $\boldsymbol{T_s} \in \mathbb{R}^m$ with entries of T_{s_i} representing the temperature of supply air to the room i.

Note that a perfect prediction of the future environmental disturbance is not possible in practice, and it results in an uncertainty in the forecasted ambient temperature, solar radiation, and other weather-related disturbances [7]. Similarly, it is difficult to capture the exact dynamical model for a complex system such as a building thermal load which results in an uncertain model for the system. For a building thermal model, both model uncertainty and prediction/forecast errors need to

be considered when defining the dynamical model for the system. This requires an appropriate model for characterizing the cumulative uncertainty resulting from inaccurate dynamical model and prediction error. Although different models exists for characterizing the uncertainty in dynamical systems [18], a majority of the recent literature concerned with MPC for home energy management models uncertainty as bounded input disturbances [7], [19], [20]. In this case, the MPC controller is implemented on the known plant model that is subjected to unknown but bounded disturbances. In this paper, we also use the bounded disturbance model.

The system dynamics after considering prediction error and model uncertainty for the building thermal model is represented as the following:

$$\boldsymbol{D}^k = \boldsymbol{d}^k + \boldsymbol{\phi}^k \tag{3}$$

$$\boldsymbol{x}^{k+1} = \boldsymbol{A}\boldsymbol{x}^k + \boldsymbol{B}\boldsymbol{u}^k \circ (\boldsymbol{T_s} - \boldsymbol{y}^k) + \boldsymbol{E}\boldsymbol{D}^k \tag{4}$$

where, ϕ^k is unknown but bounded uncertainty and represents the cumulative effects of prediction error and model uncertainty. Note that, considering the bounded uncertainty is a fair assumption. That is, based on an approximate knowledge in accuracy of modeling the building thermal model and the comparison of the actual and predicted ambient disturbances of the historical data, conservative bounds can be chosen to characterize the total effects of uncertainty on the underlying system model.

Next, we detail the equations for the power consumption of a HVAC system as a function of air mass flow rate. A typical HVAC system consumes most of its power through the heater, chiller, and fan [2]. Without loss of generality, in this paper we only consider a cooling system. The fan power consumption, $P_{f_i}^k$, is modeled as a cubic function of air mass flow rate, u_i^k.

$$P_{f_i}^k = P_{rated_i}(u_i^k/u_{rated_i})^3 \tag{5}$$

where, P_{rated_i} and u_{rated_i} are the rated power and the rated outlet air mass flow rate of the air handling unit of a HVAC system in thermal zone i, respectively; and $P_{f_i}^k$, u_i^k are power consumption and the air mass flow rate (control variable) of the fan in the thermal zone i at the sampling time k, respectively.

The cooling load is a function of the air mass flow rate, ambient temperature, and temperature of the thermal zone i as defined in [2]:

$$P_c^k = \frac{c_a}{COP} \sum_{i=1}^{m} u_i^k \left[d_p y_i^k + (1 - d_p) T_{out}^k - T_{s_i} \right] \tag{6}$$

where, T_{out}^k is the ambient temperature at sampling time k; COP is the performance coefficient of the chiller; c_a is the specific heat capacity of the air; and d_p is the instantaneous return-to-total ratio of the chiller that varies between 0 and 1.

Therefore, the total power consumption of the entire building by its HVAC system at sampling time k is given by (7).

$$P_H^k = P_c^k + \sum_{i=1}^{m} P_{f_i}^k \tag{7}$$

Discussion on Building Thermal Model Estimation Problem: A dynamic model for the building thermal load can be obtained using different model-estimation techniques such as black-box identification [21], grey-box modeling [22], and white-box modeling approach [23]. A black-box model is purely

data-driven representation for the system. A grey-box model combines the physics-based model for the system with data-driven estimation techniques for model parameters. A white-box model essentially simulates the detailed physics-based model based on the known physical properties of the system under consideration. A grey-box model combines the best of both worlds: data and physics-based model and hence is increasingly becoming more popular especially for multi-zone building simulations. A grey-box model for building thermal load first specifies the structure based on RC network topology and then identifies the model parameters from the measurements or BEPS simulations. For example, in [24], authors claim that the detailed modeling of the physical properties of building thermal load using RC modeling approach is infeasible for a multi-zone building, and propose a new approach for model-identification of a large multi-zone building. Specifically, authors in [24] simulate a physics-based model in a building simulation software that closely describes the building thermal dynamics. The identification signals were provided as inputs to the simulated model to obtain the high-quality model-identification data. We would emphasize that our proposed HVAC controller can use any of the above-mentioned model-estimation methods that derive a bilinear dynamical model for the building thermal load. The resulting bilinear model can be easily integrated with the proposed controllers to achieve an economic objective.

B. Battery Energy Storage Model

Based on [10], the dynamics for the battery energy storage can be formulated using the state-space equations for the state-of-charge (SOC) and the limits on the battery's charging and discharging power and energy as follows:

$$SOC^{k+1} = (1 - \eta)SOC^k + \rho \frac{P_{c,d}^k}{Q_{bat}} \tau \tag{8}$$

$$E^- \leqslant SOC^{k+1} \leqslant E^+ \tag{9}$$

$$-d_r \leqslant P_{c,d}^k \leqslant c_r \tag{10}$$

$$P_d^k = \begin{cases} |P_{c,d}^k| & \text{if } P_{c,d}^k < 0 \\ 0 & \text{otherwise} \end{cases} \tag{11}$$

Specifically, the battery SOC updates based on (8) where SOC^k and $P_{c,d}^k$ are the SOC and charging/discharging power of the battery at the sampling time k, respectively; η, ρ, and Q_{bat} are energy decay rate, round-trip efficiency, capacity of the battery; τ is the length of sampling time. Constraint (9) guarantees the battery SOC remains in the safety boundary where E^+ and E^- specifies bounds on the battery charging/discharging limits. Constraint (10) bounds the battery's maximum charging/discharging rates where d_r is the maximum discharge rate while c_r is the maximum charge rate. Finally, the battery discharging power is calculated in (11) and denoted by P_d^k. Also, $P_{c,d}^k > 0$ indicates that battery is charging while $P_{c,d}^k < 0$ indicates that the battery is discharging.
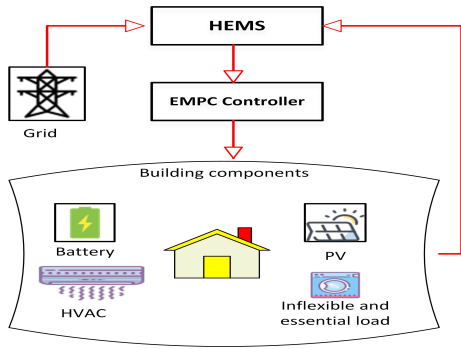
Fig. 1. System layout

C. Photovoltaic (PV) Generator Model

For the steady-state analysis, a PV generator is usually modeled as a negative constant power load with a varying load profile that depends on the solar irradiance. The PV panel is modeled as a negative load with rated active power of P_{PV}^{rated} and an associated multiplier α^k indicating the effect of variation in solar irradiance at the sampling time k. The PV generation at sampling time k, P_{PV}^k, is given by (12).

$$P_{PV}^k = \alpha^k . P_{PV}^{rated} \qquad (12)$$

Discussion: It should be noted that the proposed framework can be easily expanded to include other controllable and time-shiftable loads within the building. Since most of the controllable loads other than a HVAC system can be represented using linear dynamics, they are easy to incorporate. Moreover, the battery model can be generalized for other time-shiftable loads, such as electric vehicles (EVs) and smart dishwashers.

III. MPC FOR OPTIMAL SCHEDULING OF BUILDING'S POWER CONSUMPTION

The component layout used in this paper for a house/building is shown in Fig. 1. It is assumed that the building is equipped with the home energy management system (HEMS) [25]. HEMS has the ability to participate in the demand response program by shifting or curtailing the demand to reduce the building's energy consumption [26]. In order to satisfy the building's energy demand, HEMS can provide electricity from any combination of PV generation, battery storage, and electricity purchased from the retail electricity provider [27]. The HEMS aims at optimally co-scheduling the building's HVAC system, inflexible loads, and all available energy resources such that it can optimize the net cost of transacted energy for the specified prediction window while ensuring that the desired level of comfort is met for its occupants. The problem is formulated as an economic model predictive control (EMPC) problem with the objective of minimizing the building's total electricity usage cost for a given price vector, whose entries indicate time-of-use (TOU) electricity tariffs for each hour of the day subject to dynamical load models and load satisfaction constraints. The problem formulation is detailed below:

$$\underset{\boldsymbol{u}^k, \boldsymbol{P}_{c,d}^k}{Min} \sum_{k=t}^{t+W-1} Price^k . P_T^k + Price_b . P_d^k \qquad (13)$$

Subject to:

$$\boldsymbol{T}_{Min}^k \preceq \boldsymbol{T}_r^k \preceq \boldsymbol{T}_{Max}^k \qquad (14)$$

$$0 \leqslant P_H^k \leqslant P_{H_{Max}} \qquad (15)$$

$$\boldsymbol{u}_{Min} \preceq \boldsymbol{u}^k \preceq \boldsymbol{u}_{Max} \qquad (16)$$

$$P_T^k = P_H^k + P_l^k + P_{c,d}^k - P_{pv}^k \qquad (17)$$

$$P_T^k \geqslant 0 \qquad (18)$$

and constraints (1), (2) and (5)-(12)

The minimization of the electricity usage cost is given by the first term of (13) while the second term minimizes the battery depreciation cost. In (13), W is the prediction window, $Price_b$ is the battery depreciation cost, and P_T^k and $Price^k$ are the electric power purchased from the retail electricity provider and the electricity tariff at the sampling time k, respectively. The desired temperature range at the sampling time k, the HVAC system power consumption limits, air mass flow limits, the thermal building model, and the total consumed power by the HVAC system are presented in (14), (15), (16), (1)-(2), and (5)-(7), respectively; where variables $\boldsymbol{T}_{Min}^k, \boldsymbol{T}_{Max}^k, P_{H_{Max}}, \boldsymbol{u}_{Min}$ and $\boldsymbol{u}_{Max}$ are minimum and maximum range of the temperature ($^\circ C$) at the sampling time k, maximum HVAC power consumption limits, minimum and maximum limits for HVAC mass flow rate, respectively. Constraint (17) determines the total power consumption where P_l^k is the consumed power by inflexible loads of the building at the sampling time k. Note that we use element-wise operation sign in (14) and (16) for comparing the corresponding variables of each thermal zone (e.g. $T_{Min,i}^k \leqslant T_{r,i}^k \leqslant T_{Max,i}^k$). Also $\boldsymbol{u}_{Min}$ and $\boldsymbol{u}_{Max}$ are the the vectors with the same size as $\boldsymbol{u}^k$ whose entries are equal to u_{Min} and u_{Max}, respectively. Lastly, constraint (18) states that the total power consumption cannot be negative; in other words, the surplus of energy cannot be sold back to the power grid.

It should be noted that (1) is bilinear in system inputs and outputs, which results in a nonlinear economic model-predictive control (NL-EMPC) problem[1]. Due to the expensive computations required to solve the NL-EMPC problem, Jacobian-linearization methods are used extensively in the related literature. This approach is based on linearizing the original bilinear system around an equilibrium point. The equilibrium point of (1) is obtained by setting the indoor room temperature equal to the desired room temperature specified by the building's occupants also called set-point temperature [17]. The linearized model then tracks the set-point temperature using MPC technique. The system dynamics for the building thermal load using Jacobian linearization is formulated in (19).

$$\boldsymbol{x}^{k+1} = \boldsymbol{A}\boldsymbol{x}^k + \boldsymbol{B}\boldsymbol{u}^k \circ (\boldsymbol{T_s} - \boldsymbol{T}_{set}) + \boldsymbol{E}\boldsymbol{D}^k \qquad (19)$$

where $\boldsymbol{T}_{set} \in \mathbb{R}^m$ with entries of $T_{set,i}$ which represents the set-point temperature of the room i. Note that using this approach, the value of each term (for each room) of the vector $(\boldsymbol{T_s} - \boldsymbol{T}_{set})$ is a constant number; thus, (19) and (2) are in the form of linear state space equations. Although this method shows good results for set-point temperature tracking applications, it is not a valid approach when optimizing an economic objective which is the focus of this paper. That is, Jacobian-linearization is not valid when set-point temperatures

---

[1]Equations (1) and (4) are equivalent when there is no uncertainty.
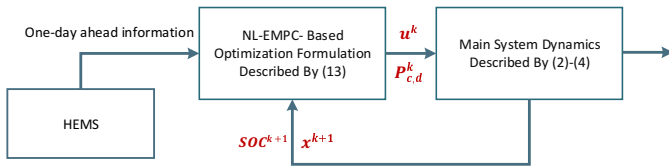
Fig. 2. Schematic for NL-EMPC controller

can vary over a wide-range due to varying occupancy patterns when attempting to optimize electricity usage for time-varying cost of electricity. To address the above problem, in this paper we propose two EMPC methods. First, we solve this problem by using a full Nonlinear-EMPC (NL-EMPC) model that involves the nonlinear dynamical model for building thermal loads. Next, we propose a novel Linearized-EMPC (L-EMPC) model that is not only computationally efficient with improved processing time, but also mimics the behavior of the illustrated NL-EMPC model by accurately representing the system dynamics. Our approach for linearization is inspired by feedback-linearization methods widely used in the controls-engineering community.

Discussion on the Nonlinear Battery Model: The current formulation for the battery is nonlinear and adds computational complexity to the problem. When the depreciation cost of the battery is low and negligible (determined by battery manufacturing cost and battery maximum charging/discharging cycles), the constraint (11) and second term of objective function (13) can be eliminated. This approximation leads to a linear state-space equation for the battery storage system. When the depreciation cost is high, the non-linearity in the battery storage model due to (11) can be relaxed using binary variables as explained in the Appendix Section A. Note that we refer to constraint (11) in the following discussions for the ease of use; however, we use the constraints provided in the Appendix Section A in simulations.

A. Nonlinear Economic Model Predictive Controller

A schematic view of the proposed NL-EMPC is detailed in Fig. 2. At the beginning of each day, HEMS provides the NL-EMPC controller with one-day ahead prediction information including the occupancy pattern, environmental disturbances, PV generation, forcasted power consumption by inflexible loads, and TOU prices for the next 24 hours of the day. This information determines d^k in (1), T_{Min}^k and T_{Max}^k in (14), P_{pv}^k and P_l^k in (17), and $Price^k$ in objective function (13). The NL-EMPC algorithm solves the minimization problem (13), with constraints (1), (2), (5)-(12) and (14)-(18) at each sampling time k. This results in optimal mass air flow rate trajectory $[u^t, u^{t+1}, ..., u^{t+W-1}]$ and battery charging/discharging trajectory $\left[P_{c,d}^t, P_{c,d}^{t+1}, ..., P_{c,d}^{t+W-1} \right]$ for a prediction window from time t to time $t+W-1$. After obtaining the optimal mass air flow rate and charging/discharging trajectories, only the first entry of these trajectories (u^t and $P_{c,d}^t$) are applied to the building thermal dynamics under the effects of uncertainty and the battery charging/discharging equations stated by [(2), (4)] and (8), respectively, to control the HVAC system and battery operation. After observing the new values of the building thermal states (x^{t+1}) and SOC^{t+1}, the NL-EMPC algorithm moves one step forward and uses the observed values as

the new initial condition for the next step. The minimization problem is solved again for time intervals from $t+1$ to $t+W$. The same process continues for the next time-steps, and a constrained optimization problem is solved repeatedly over a moving time horizon to obtain the optimal control actions using predictions of future costs and disturbances. This control method is also known as *receding horizon control approach.* Note that when all the states cannot be measured, an observer should be designed to predict the state variables [28]. The design of the observer is, however, outside of the scope of this paper.

B. Linearized Economic Model Predictive Controller

In this section, we propose a novel linearized model for economical control of a buildings' HVAC system while considering other necessary loads and multiple of energy sources for a building as explained in the Section III-A. Notice that the nonlinearity in NL-EMPC described in Section III-A arise from: (a) bilinear term in second term of the constraint (1) due to product of its elements in the form of u_i^k and y_i^k ; (b) cubic control input term $(u_i^k)^3$ in (5) for a fan power; and (c) bilinear product of control input and output variables, $u_i^k.y_i^k$, in (6) for chiller power. First, an exact linear model for the dynamical HVAC system model is obtained using a feedback linearization technique. Next, the nonlinear relationship between power consumption of a fan and a chiller with the air mass flow rate is linearized using approximation techniques. This results in a linear EMPC (L-EMPC) formulation that can be solved using off-the-shelf linear optimization tools. The resulting model is not only computationally efficient but also closely approximates the nonlinear plant dynamics for the HVAC system.

1) Feedback Linearization of Bilinear HVAC Dynamics: Notice that the state-space model described in (1)-(2) is nonlinear due to bilinearity of constraint (1). To handle non-linearity in (1), feedback linearization is proposed in this section where by finding an explicit relation between the system output y^k and the control input u^k, we cancel out the non-linearity of the system. Interested readers can refer to [29] for further details regarding feedback linearization approaches.

To linearize (1), we define the following equation:

$$v^k = u^k \circ (T_s - y^k) \qquad (20)$$

where $v^k \in \mathbb{R}^m$ is the vector of new input variables at sampling time k after feedback linearization whose elements (v_i^k) are new input variables for thermal zone i. Then, using (20) in (1), we obtain:

$$x^{k+1} = Ax^k + Bv^k + Ed^k \qquad (21)$$

It should be noted that in (21), state vector x^k remains the same as the one in (1), and as the result the equation (2) describes the output for the building thermal model after implementing the feedback linearization approach.

Note that since (21) is based on the new control input vector, the minimization problem defined in (13) should be changed accordingly. The following equation defines the minimization of electricity usage cost obtained after feedback linearization:

$$\underset{v^k}{Min} \sum_{k=t}^{t+W-1} Price^k.P_T^k \qquad (22)$$

The next step is to map the constraints (5)-(7) and (16), which are based on $\boldsymbol{u}^k$ to the new input variables $\boldsymbol{v}^k$ as detailed in the following section.

2) Mapping Input Constraints: In this section, we address the mapping of constraint (16) to the new input variable $\boldsymbol{v}^k$. The mapping problem, at each sampling time k, can be defined as deriving the constraint of the following form:

$$\boldsymbol{v}_{Min}^{k+j|k} \preceq \boldsymbol{v}^{k+j|k} \preceq \boldsymbol{v}_{Max}^{k+j|k} \ \text{ for } j = 0, 1, ..., W-1 \qquad (23)$$

where $\boldsymbol{v}^{k+j|k}$ is the value of L-EMPC control input vector $\boldsymbol{v}^{k+j}$ (for future time $k+j$) obtained at sampling time k; $\boldsymbol{v}_{Min}^{k+j|k}$ and $\boldsymbol{v}_{Max}^{k+j|k}$ are the minimum and maximum limit for control input $\boldsymbol{v}^{k+j}$ obtained at sampling time k, respectively[2]. Finding the bounds of the new control input in constraint (23) requires to solve the following optimization problem at each sampling time k:

$$\begin{aligned} \boldsymbol{v}_{Min}^{k+j|k} &= \underset{\boldsymbol{u}^{k+j|k}}{Min} [\boldsymbol{u}^{k+j|k} \circ (\boldsymbol{T_s} - \boldsymbol{y}^{k+j|k})] \\ \boldsymbol{v}_{Max}^{k+j|k} &= \underset{\boldsymbol{u}^{k+j|k}}{Max} [\boldsymbol{u}^{k+j|k} \circ (\boldsymbol{T_s} - \boldsymbol{y}^{k+j|k})] \end{aligned} \qquad (24)$$

subject to

$$\boldsymbol{u}_{Min} \preceq \boldsymbol{u}^{k+j|k} \preceq \boldsymbol{u}_{Max} \ \text{ for } j = 0, 1, ..., W-1$$

where $\boldsymbol{u}^{k+j|k}$ and $\boldsymbol{y}^{k+j|k}$ represent the input $\boldsymbol{u}^{k+j}$ and output $\boldsymbol{y}^{k+j}$ computed at the sampling time k. Then, by substituting $j = 0$ in (24), bounds for the input control at the current sampling time can be calculated as:

$$\begin{aligned} \boldsymbol{v}_{Min}^{k|k} &= \underset{\boldsymbol{u}}{Min} \ \boldsymbol{u}^k \circ (\boldsymbol{T_s} - \boldsymbol{y}^k) \\ \boldsymbol{v}_{Max}^{k|k} &= \underset{\boldsymbol{u}}{Max} \ \boldsymbol{u}^k \circ (\boldsymbol{T_s} - \boldsymbol{y}^k) \end{aligned} \qquad (25)$$

subject to

$$\boldsymbol{u}_{Min} \preceq \boldsymbol{u}^k \preceq \boldsymbol{u}_{Max}$$

As is clear, this optimization problem is trivial to solve due to affine objective function in u_i^k [30]. On the other hand, it is difficult to compute the constraints for future input over the prediction window $[\boldsymbol{v}^{k+1|k}, \boldsymbol{v}^{k+2|k}, ..., \boldsymbol{v}^{k+W-1|k}]$. Note that in order to solve the optimization problem formulated in (24) to obtain the mapped constraints in (23), the estimates of the future values of input and output variables are needed. However, these estimates are not available until the L-EMPC problem is solved that in turn requires the mapped input constraints in (23) over the entire prediction window [31]. To address this problem, we use a similar but slightly modified approach illustrated in [32] described as follows.

At the first sampling time of solving the problem ($k = 0$), we use the constant input constraints to calculate the bounds on future control input in prediction window W as follows:

$$\begin{aligned} \boldsymbol{v}_{Min}^{k+j|k} &= \boldsymbol{v}_{Min}^{k|k} \\ \boldsymbol{v}_{Max}^{k+j|k} &= \boldsymbol{v}_{Max}^{k|k} \end{aligned} \qquad (26)$$

$$\text{for } j = 0, 1, 2, ..., W-1$$

where $\boldsymbol{v}_{Min}^{k|k}$ and $\boldsymbol{v}_{Max}^{k|k}$ are obtained based on (25). Hence, the L-EMPC uses (25) and (26) to solve the optimization

problem formulated in (22) at the first sampling time ($k = 0$). Then, for solving the problem at each of the next sampling times ($k = 1, 2, ..., W-1$), we use inputs calculated from the previous sampling time to calculate the future constraints at the current sampling time. The resulting problem is formulated as the following:

$$\begin{aligned} \boldsymbol{v}_{Min}^{k+j|k} &= \underset{\boldsymbol{u}^{k+j|k}}{Min} [\boldsymbol{u}^{k+j|k-1} \circ (\boldsymbol{T_s} - \boldsymbol{y}^{k+j|k-1})] \\ \boldsymbol{v}_{Max}^{k+j|k} &= \underset{\boldsymbol{u}^{k+j|k}}{Max} [\boldsymbol{u}^{k+j|k-1} \circ (\boldsymbol{T_s} - \boldsymbol{y}^{k+j|k-1})] \end{aligned} \qquad (27)$$

subject to:

$$\boldsymbol{u}_{Min} \preceq \boldsymbol{u}^{k+j|k} \preceq \boldsymbol{u}_{Max} \ \text{ for } j = 1, ..., W-1$$

In (27), for each thermal zone i and for each $j = 1, ..., W-1$, if $(T_{s_i} - y_i^{k+j|k-1}) > 0$, then u_{Min} and u_{Max} determines $v_{Min,i}^{k+j|k}$ and $v_{Max,i}^{k+j|k}$, respectively; otherwise u_{Min} and u_{Max} determines $v_{Max,i}^{k+j|k}$ and $v_{Min,i}^{k+j|k}$, respectively. Note that bounds for the control input at $j = 0$ are obtained based on (25).

3) Linearized Power Consumption Model for HVAC: As previously mentioned, constraints (5), (6) and consequently (7) introduced in Section II-A are based on $\boldsymbol{u}^k$. After using feedback linearization technique, these should be redefined based on the L-EMPC control input, $\boldsymbol{v}^k$.

First, we consider constraint (5). By modifying constraint (20) at each sampling time k, we obtain $\boldsymbol{u}^k$ based on $\boldsymbol{v}^k$ over the prediction window in (28).

$$\boldsymbol{u}^{k+j|k} = \frac{\boldsymbol{v}^{k+j|k}}{\boldsymbol{T_s} - \boldsymbol{y}^{k+j|k}} \ \text{ for } j = 0, 1, ..., W-1 \qquad (28)$$

where for each sampling time k and for each j, each entry of the right hand-side of the above equation is defined as $\frac{v_i^{k+j|k}}{T_{s_i} - y_i^{k|k+j}}$. Substituting (28) in (5), we obtain the following:

$$P_{f_i}^{k+j|k} = P_{rated_i} \left(\frac{v_i^{k+j|k}}{(T_{s_i} - y^{k+j|k})u_{rated_i}} \right)^3 \ \text{ for } j = 0, ...W-1 \qquad (29)$$

where $P_{f_i}^{k+j|k}$ is the total fan power consumption computed at the sampling time k in thermal zone i. Although (29) is based on the input variable of the L-EMPC, it is non-linear due to the cubic relation between $P_{f_i}^{k+j|k}$ and $v_i^{k+j|k}$, and inverse-polynomial relation between $P_{f_i}^{k+j|k}$ and $y_i^{k+j|k}$; hence, it cannot be directly integrated into the L-EMPC model. To eliminate the nonlinearity between $P_{f_i}^{k+j|k}$ and $y_i^{k+j|k}$, we use the same method we previously proposed in Section III-B2 for mapping input constraints as detailed below.

For the first sampling time ($k = 0$), we consider the initial value as $\boldsymbol{y}^0 \in \mathbb{R}^m$ (with entries of y_i^0 for the vector $\boldsymbol{y}^k$), and set it as the value of the output for the rest of the sampling time in the prediction window as follows:

$$\boldsymbol{y}^{k+j|k} = \boldsymbol{y}^0 \ \text{ for } j = 0, 1, ..., W-1 \qquad (30)$$

Then, for the next sampling times in the prediction window, (e.g. $k = 1, 2, ..., W-1$), we use the output calculated at the previous sampling time, $\boldsymbol{y}^{k+j|k-1}$ as the future outputs at the current sampling time, $\boldsymbol{y}^{k+j|k}$, stated as the following:

$$\boldsymbol{y}^{k+j|k} = \boldsymbol{y}^{k+j|k-1} \ \text{ for } j = 0, 1, ..., W-1 \qquad (31)$$

Note that in (31) $y_i^{k|k} = y_i^{k|k-1}$. This implies that current value of the output which obtained at the previous sampling time $(k-1)$ is used as the initial condition for solving the problem at the current sampling time (k). For example at the current sampling time (e.g. 12:00), we use the temperature of this time as the initial condition to find the temperature for the next sampling time (e.g. 12:15). Using this approach, future output variables $y_i^{k+j|k}$ are constant and equal to the output variables obtained at the previous sampling time. This approach, there-fore, makes $y_i^{k+j|k}$ constant at sampling time k and eliminates the inverse-polynomial relation between $P_{f_i}^{k+j|k}$ and $y_i^{k+j|k}$. Although approximate, this method successively improves the prediction of output variables at the current sampling time.

Note that (6) is also nonlinear due to the product of variables in form of $u_i^k . y_i^k$. This imposes the term $v_i^k . y_i^k$ in the equivalent chiller equation after feedback linearization. This nonlinearity is also relaxed using the same approach proposed at the beginning of this section by modifying $\boldsymbol{y}^{k+j|k}$ based on (30) and (31). Thus, for the first sampling time $(k = 0)$, this can be written as follows:

$$P_c^{k+j|k} = \frac{c_a}{COP} \sum_{i=1}^{m} \left(\frac{v_i^{k+j|k}}{T_{s_i} - y_i^0} \right) \left(d_p y_i^0 + (1 - d_p)T_{out}^k - T_{s_i} \right) \quad (32)$$

$$\text{for } j = 0, 1, 2, ..., W - 1$$

Then, for the next sampling times in the prediction window $(k = 1, 2, ..., W - 1)$, the formulation is changed as follows:

$$P_c^{k+j|k} = \frac{c_a}{COP} \sum_{i=1}^{m} \left(\frac{v_i^{k+j|k}}{T_{s_i} - y_i^{k+j|k-1}} \right) \cdot \left(d_p y_i^{k+j|k-1} + (1 - d_p)T_{out}^k - T_{s_i} \right) \quad (33)$$

$$\text{for } j = 0, 1, 2, ..., W - 1$$

Next, we employ the incremental approach of piecewise lin-earization to relax the nonlinearity in $\boldsymbol{P}_f^{k+j|k}$ due to cubic term of $\boldsymbol{v}^{k|k+j}$. The approach is explained briefly here; however, interested readers can refer to [33] for further details on the piecewise linearization approach.

At each sampling time, we approximate each $v_i^{k+j|k}$ in (29) as the summation of multiple line segments. In order to formulate the linear approximated function, we first introduce following two conditions [33]:

- The line segments in $\mathbf{L}$ can be ordered as $l_1, l_2, ..., l_\mathbf{L}$ subject to $l_x \cap l_{x-1} \neq \emptyset$ for $x \in \{2, ..., |\mathbf{L}|\}$, where operator $|.|$ shows the number of the elements.
- For the order in $\mathbf{L}$, the vertices of each line segment l_x ordered as h_x^0 and h_x^1 for $x \in \{2, ..., |\mathbf{L}|\}$.

At each sampling time, the limits of the linearized control input specified by (23) determines the initial vertex of the first line segment (h_1^0) and ending vertex of the last line segment $(h_\mathbf{L}^1)$. Then, by introducing auxiliary continuous variables σ_x, which can be interpreted as the slopes of line segments l_x with the vertices h_x^0 and h_x^1 for $x \in \{1, ..., |\mathbf{L}|\}$, we can define the piecewise linearized input v_i^k as follows:
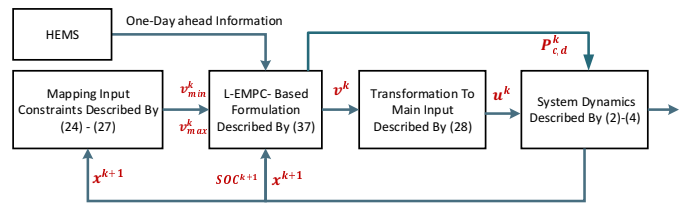
Fig. 3. Schematic for the Proposed L-EMPC controller

$$v_i^k = h_1^0 + \sum_{x=1}^{|\mathbf{L}|} \sigma_x (h_x^1 - h_x^0)$$

$$f(v_i^k) = f(h_1^0) + \sum_{x=1}^{|\mathbf{L}|} \sigma_x [f(h_x^1) - f(h_x^0)] \quad (34)$$

$$\sigma_x \geqslant 0 \text{ for } x \in \{1, ..., |\mathbf{L}|\}$$

where $f(.) = (.)^3$ for any arbitrary value of $(.)$ in (34). Note that, as $(v_i^k)^3$ is monotonically increasing function, there is no need for binary variables to define piecewise linear model. Using (30), (31) and (34), we linearize (29) for the first sampling time $(k = 0)$ as following:

$$P_{f_i}^{k+j|k} = P_{rated_i} \left(\frac{1}{(T_{s_i} - y_i^0)u_{rated_i}} \right)^3 f(v_i^{k+j|k}) \quad (35)$$

$$\text{for } j = 0, 1, 2, ..., W - 1$$

Then, for the next sampling times in the prediction window $(k = 1, 2, ..., W - 1)$, the formulation is changed as follows:

$$P_{f_i}^{k+j|k} = P_{rated_i} \left(\frac{1}{(T_{s_i} - y_i^{k+j|k-1})u_{rated_i}} \right)^3 f(v_i^{k+j|k}) \quad (36)$$

$$\text{for } j = 0, 1, 2, ..., W - 1$$

Finally, the formulation for L-EMPC is detailed in (37).

$$\underset{\boldsymbol{v}^k}{Min} \sum_{k=t}^{t+W-1} Price^k . P_T^k \quad (37)$$

Subject to:

$$\boldsymbol{x}^{k+1} = \boldsymbol{A}\boldsymbol{x}^k + \boldsymbol{B}\boldsymbol{v}^k + \boldsymbol{E}\boldsymbol{d}^k$$

$$\boldsymbol{y}^k = \boldsymbol{C}\boldsymbol{x}^k$$

$$\boldsymbol{v}_{Min}^{k+j|k} \preceq \boldsymbol{v}^{k+j|k} \preceq \boldsymbol{v}_{Max}^{k+j|k}, \text{ for } j = 0, 1, ..., W - 1$$

$$\boldsymbol{T}_{Min}^k \preceq \boldsymbol{T}_r^k \preceq \boldsymbol{T}_{Max}^k$$

$$0 \leqslant P_H^k \leqslant P_{H_{Max}}$$

$$P_H^k = P_c^k + \sum_{i=1}^{m} P_{f_i}^k$$

$$P_T^k = P_H^k + P_l^k + P_{c,d}^k - P_{pv}^k$$

$$P_T^k \geqslant 0$$

constraints (8)-(12), (20), (24)-(27) and (30)-(36).

The L-EMPC problem is illustrated in Fig. 3. At the beginning of each day, the HEMS provides the L-EMPC controller one-day ahead prediction information as illus-trated in Section III-A. Then, using this information and mapped input constraints defined in (24), the L-EMPC solves the optimization problem in (37) at each sampling time k. The results of solving this optimization problem

is the vector of feedback linearized input optimal trajectory $[\boldsymbol{v}^t, \boldsymbol{v}^{t+1}, \boldsymbol{v}^{t+2}, ..., \boldsymbol{v}^{t+W-1}]$ and the battery charging/discharging trajectory $[P_{c,d}^t, P_{c,d}^{t+1}, ..., P_{c,d}^{t+W-1}]$. The first entry of linearized control input trajectory $(\boldsymbol{v}^t)$ is used to find the value of current air mass flow rate $(\boldsymbol{u}^t)$ based on (28). Finally, same as the receding horizon approach for the NL-EMPC controller, $\boldsymbol{u}^t$ and first entry of battery charging/discharging trajectory $(P_{c,d}^t)$ are applied to the building thermal dynamic model and the battery charging/discharging equations stated by [(2) and (4)] and (8), respectively, to control the HVAC system and the battery operation. The measured values of the states $(\boldsymbol{x}^{t+1})$ and SOC^{t+1} are used as the initial values in the next sampling time and the same algorithm continues.

Discussion on the Effects of Uncertainty on Control Decisions: In the related literature, robust MPC has been proposed for controlling dynamical systems with uncertainties. A robust MPC controller essentially generates optimal control decisions by solving a stochastic optimization/control problem that implicitly includes the effects of uncertainty in control decisions. Min-max [34], Tube-based [35] and multi-stage approach [36] are common methods employed for designing a robust economic model predictive controller (REMPC). Unfortunately, using aforementioned methods lead to conservative control decisions resulting in a higher cost when optimizing an economic objective function. Thus, REMPC formulations may degrade the economical benefits when to compared to the nominal EMPC models. Another drawback of using common REMPC approaches is the added computational complexity; this is specially a critical concern for our problem where prediction window is 24 hours ahead in 15 minute intervals (96 sampling times). Therefore, a robust version may not be computationally tractable for the problem at hand.

In this paper, we model nominal the L-EMPC and the NL-EMPC to control the system of interest while considering the effects of the uncertainty on system dynamics. Note that, in the presence of uncertainty, the actual trajectory obtained using nominal MPC/EMPC methods will deviate from the optimal trajectory. The two factors that contribute to the deviation from optimal control trajectory for the associated controller are attributed to the errors in the model estimation and errors in environmental disturbances prediction. Note that considering small model uncertainty for the thermal building model is a valid assumption. That is, as is proposed in [20], at each sampling time and before using the building thermal model for control purposes, time-varying parameters of the building can be tuned based on adaptive approaches such as Kalman filter or/and observer in an online fashion from the measurements of the previous sampling time. The results in [20] show that using this approach decreases uncertainty in the thermal building model dramatically and consequently provides an acceptable model for the building thermal load. Furthermore, the environmental disturbances usually have a forecast accuracy of more than 90% for one-day ahead of time [37]. Thus, the error in the day ahead prediction of environmental disturbances (d^k) has a negligible effect on the dynamics of the building thermal model. Therefore, it

(a) Ambient Temperature

(b) TOU electricity tariffs

(c) Received occupancy patterns at the beginning of the day
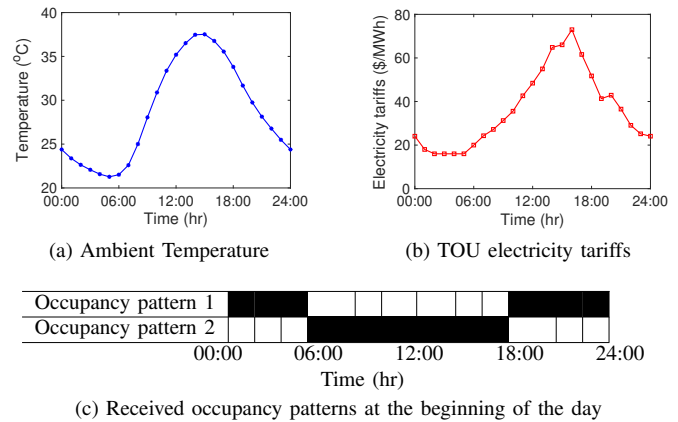
Fig. 4. Model Parameters used for a building's HVAC system

can be claimed that a nominal EMPC model for building thermal loads provides the computational advantage while not significantly deteriorating the control decisions due to the uncertainty. Lastly, designing a computationally tractable robust controller that can provide the economical benefits is a separate problem and is not within the scope of this work.

IV. RESULTS AND DISCUSSIONS

In this section, we conduct a set of experiments to validate the efficiency of the proposed L-EMPC controller by benchmarking the results against an equivalent NL-EMPC controller; then, we show the weakness of conventional methods for solving the introduced problem in this paper. For the thermal building model, we consider a thermal zone with 7 states (four states for temperature of walls, two states for temperature of floor and ceiling, and one state for indoor thermal zone temperature) with the parameters the same as [2]. Other building parameters are: $COP = 3$, $d_p = 0$, $T_s = 10$ (°C), $T_{set} = 23$ (°C) (for Jacobian-linearized model), P_{rated} and u_{rated} are $600W$ and $1kg/s$, respectively. The parameters for the battery energy storage system are as follows: $\eta = 0, \rho = 1, E^- = 0.25, E^+ = 1, d_r = c_r = 1kW$ and $Q_{bat} = 3kWh$. The predicted ambient temperature, the 24-hour TOU electricity tariffs and occupancy patterns for the building received at the beginning of the day are shown in Fig. 4. The occupancy patterns represent the typical cases for residential (occupancy pattern 1) and commercial (occupancy pattern 2) buildings. To maintain the desired comfort level of building occupants, it is assumed that during occupancy, the indoor temperature in building should lie between 21- 25 (°C), otherwise, there is no limit for the thermal zone temperatures. There are no temperature limits for the other 6 states of the thermal zones for all the times.The initial temperature of all 7 states of the building with occupancy pattern 1 are 24 (°C), while these values are changed to 28 (°C) when the building follows the occupancy pattern 2. The simulations are done on a dual core i7 3.41 GHz processor with 16 GB of RAM.

A. *Validity of proposed approach for HVAC control*

This section aims at validating the proposed L-EMPC and NL-EMPC when controlling only the building's HVAC system. Therefore, we set $P_l^k = P_{c,d}^k = P_{pv} = 0$ in (17), and remove the battery and PV constraints in (8)-(12) from
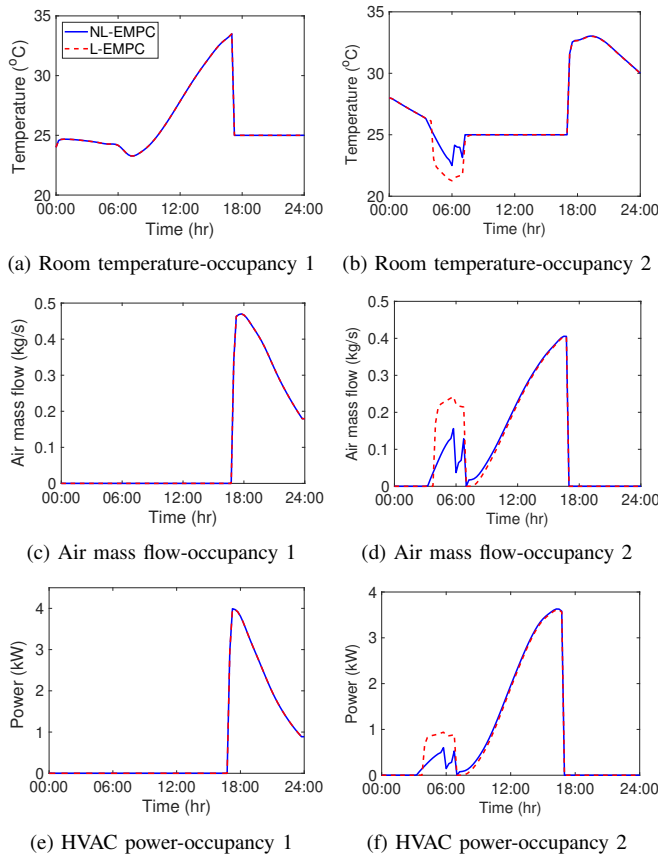
Fig. 5. Comparison of NL-EMPC and L-EMPC controllers based on internal zone temperature, air mass flow and HVAC power consumption for defined occupancy patterns.

problem formulations in Section III for both NL-EMPC and L-EMPC controllers. The resulting problem aims to minimize the current and future cost of energy consumption by the HVAC system. All essential constraints are included in the rest of the test cases.

Starting at the beginning of a day (00:00) and after receiving one-day ahead information, both controllers solve the EMPC optimization problem for the next 24 hours at a sampling rate of 15 minutes as described in Sections III-A and III-B.

For both occupancy patterns and both EMPC controllers, Fig. 5 shows the evolution of indoor building temperature, optimal value of the control input u (air mass flow rate) and the HVAC system power consumption. As is seen in Fig. 5c and Fig. 5d, when the building is occupied, the controllers adjust the air mass flow rate of the HVAC cooling system such that the temperature of the building lies within the prespecified comfort range (see Fig. 5a and Fig. 5b) while simultaneously minimizing the cost of transacted energy. On the contrary, when there is no occupancy in the building, controllers minimize the total cost of energy usage by turning the HVAC cooling system off. Note that there are times during the day (e.g. 00:00-06:00 for the occupancy pattern 1) that although the building is occupied, there is no need to utilize the HVAC system ($u = P_H = 0$) to set the indoor temperature in a desirable range (21- 25 °C). That is, the ambient temperature at these times is low and sufficient to maintain the thermal-

zone temperature within the occupants' comfort level without requiring the HVAC cooling system. The price-sensitivity of the model is emphasized for the optimal controls obtained for the occupancy pattern 2. Notice that although the building is unoccupied till 6:00, the HVAC system control is ON from 4:00-6:00. That is, due to the low TOU electricity tarrifs, the optimal solution is to precool the building from 4:00-6:00 by turning ON the HVAC system, so as to consume a smaller amount of expensive electricity after 6:00. Both NL-EMPC and L-EMPC are price-responsive and leverage the thermal building dynamics to minimize the overall cost of transacted energy.

Another interesting observation for the occupancy pattern 2 is the rapid change of the room temperature from 25 °C at 18:00 to 31.58 °C at 18:15 (during one sampling time). That is, based on the heat transfer equations of the thermal building model nodes and the consequent thermal building space state model (see [17] for more details), the room temperature is evolved and influenced by the temperatures of all other nodes in the thermal building model, control input and disturbances. Note that the air mass flow is applied directly to change the room temperature (although the walls' temperatures are influenced by the room temperature and hence indirectly from the air mass flow). Thus, before 18:00, although the room's temperature is kept within the comfort range of its occupants by applying the control input of the HVAC system (air mass flow) to the room, walls have relatively higher temperatures at this time, as there is no constraint in any time of the day for the walls' temperatures. As the result, at 18:00 when the optimal control action for the EMPC controllers is to turn the HVAC system off, the room temperature is affected by walls' temperatures and increases to a relatively high value in a short time-period.

Note that although the ambient temperature is the most important disturbance that affects the room temperature, it is not always the dominant factor and there are other components (e.g. solar irradiation) in the vector $\boldsymbol{d}^k$ that can affect the thermal building nodes' temperatures as well. Therefore, temperatures of some walls are increased[3] at some intervals of the day (e.g 14:30-18:00) despite of decrease in the the ambient temperature. This also explains the increase of the HVAC power consumption after 14:30 for the occupancy pattern 2 despite of a decrease in the the ambient temperature. The EMPC is a model-based controller and it considers the prediction of disturbances and dynamics of the system for calculating the optimal trajectory of the system's input ($\boldsymbol{u}^k$). Hence, to maintain the comfort-level while minimizing the cost, the optimal solution is to increase the air mass flow rate for the HVAC system to cool the walls as their temperatures have a direct impact on the room temperature. This avoids purchasing a high volume of expensive energy later during the day.

Next, Table I details the comparison of NL-EMPC and L-EMPC controllers in terms of optimal cost and computation

---

[3]The changing position of the sun through the day affects the radiation. Also, it should be noted that walls and the roof are not affected equally from the solar irradiation during the day. In this paper, due to lack of the data, we use a sinusoidal input for the sun irradiation related elements in $\boldsymbol{d}^k$.

TABLE I
SIMULATION DETAILS OF L-EMPC AND NL-EMPC

Approach	Occupancy Pattern	Cost($)	Time(s)	Solver
NL-EMPC	Occupancy pattern 1	0.7651	6109	MATLAB-IPOPT
	Occupancy pattern 2	1.1041	8628	
L-EMPC	Occupancy pattern 1	0.7651	35	MATLAB-linprog
	Occupancy pattern 2	1.1078	37	

time for both occupancy patterns. We use IPOPT and linprog functions in MATLAB to solve NL-EMPC and L-EMPC models, respectively. As is seen, there is a negligible difference in cost function obtained using NL-EMPC and L-EMPC controllers while the L-EMPC controller significantly improves the simulation time. Note that although for the occupancy pattern 1, there is a negligible difference in cost of energy usage for the NL-EMPC vs. the L-EMPC for the occupancy pattern 2, the NL-EMPC results in slightly lower cost of energy usage. Although the optimal costs differ, from Fig. 5, it can be concluded that the L-EMPC is price-responsive and closely mimics the solutions derived from the NL-EMPC controller. Furthermore, the L-EMPC leads to approximately 200 times improvement in the computation speed, making it more suitable for real-time control of buildings' HVAC systems.

It is interesting to observe that the L-EMPC optimal decisions match exactly with the NL-EMPC decisions for the occupancy pattern 1 but not for the occupancy pattern 2. The reason for this difference in the L-EMPC accuracy is attributed to the approach used for mapping the constraints in feedback linearized model for bilinear dynamical model for the building thermal loads. Recall that this constraint mapping is output dependent and requires an estimate of the output variable trajectory to solve the L-EPMC model for the current sampling time. Note that these estimates are not available until the L-EMPC problem is solved. We use a prediction based approach to solve this problem. That is, at every sampling interval, we use an estimate of future output trajectory and solve for the control decisions and output trajectory using the L-EMPC model. For the next sampling interval, we use the output trajectory obtained in the previous time step as the new estimate for output variable trajectory. This approach successively improves our estimates of output trajectory thus improving the consequent control decisions and bringing those closer to the NL-EMPC control decisions. For the occupancy pattern 1, since the optimal decisions are simply turning the HVAC off when the building is not occupied and tracking the 25 ($^\circ C$) (upper bound for the specified occupant's comfort level), the future prediction exactly matches the actual output trajectory. Thus, the L-EMPC exactly represents the NL-EMPC model. However, for the occupancy pattern 2, the optimal decision is to leverage the TOU prices to over-cool the building between 4-6 am and use that energy later when the building is occupied (after 6 am). In this case, the prediction of the output provided at earlier time steps does not exactly represent the actual future output trajectory that leverages the TOU prices. Hence, the L-EMPC model successively improves the future trajectory by learning more about the economical benefits of overcooling the system in this setting. This is the reason L-EMPC does not exactly track and only approximate the NL-EMPC control trajectory for the duration when price-responsiveness of the

(a) Room temperature-occupancy 1   (b) Room temperature-occupancy 2

(c) Occupancy pattern 1   (d) Occcupancy pattern 2

(e) HVAC power-occupancy 1   (f) HVAC power-occupancy 2
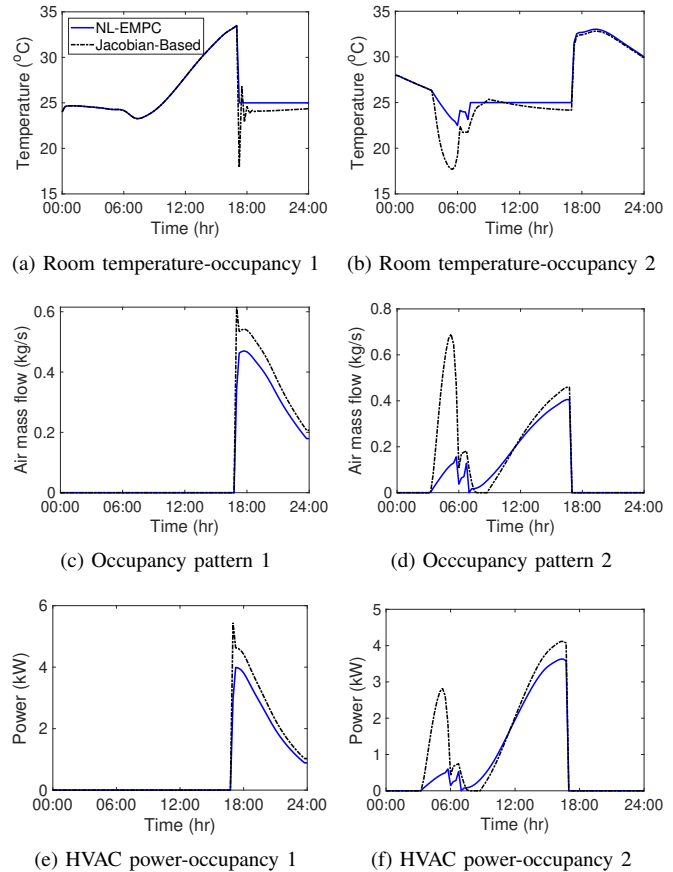
Fig. 6. Comparison of bilinear building thermal model and Jacobian-linearized building thermal model for optimal control decisions using NL-EMPC based on internal zone temperature, air mass flow and HVAC power consumption for defined occupancy patterns.

building thermal model is being leveraged.

B. Jacobian-Linearized vs. Bilinear Building Thermal Model

As it was mentioned in Section III, using Jacobian linearization method leads to controlling an inaccurate thermal building model and consequently undesirable results. The effect of Jacobian linearization can be demonstrated by substituting (19) for (1) in the NL-EMPC formulation (13). Thus, the NL-EMPC problem is solved based on both thermal building models to ensure that the experiment only captures the effect of Jacobian linearization on control decisions.

Fig. 6 compares NL-EMPC controller based on the Jacobian-linearized and the bilinear thermal building models for internal zone temperature, air mass flow and HVAC power consumption for defined occupancy patterns. On comparing the air mass flow trajectories derived using different occupancy patterns, Figs. 6c and 6d show that using Jacobian-linearized building thermal model leads to undesirable control actions. The effect of these control actions can be seen in Fig. 6b where there are violations in occupants comfort-level (e.g. 09:15 for the occupancy pattern 2). Furthermore, Figs. 6e and 6f show that using the controller based on the Jacobian-linearized thermal building model leads to more power consumption compared to the NL-EMPC controller and increases the cost of energy usage to $0.9177 and $1.2632 from $0.7651
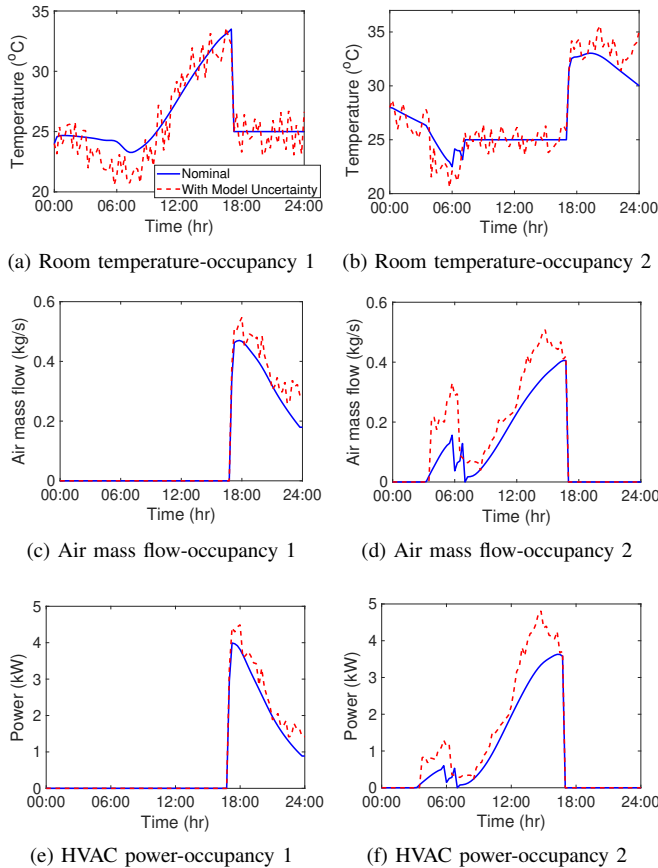
Fig. 7. Effect of uncertainty based on internal zone temperature and air mass flow for defined occupancy patterns.

and \$1.1041 per day for the occupancy patterns 1 and 2, respectively.

C. Effect of Model Uncertainty for L-EMPC Controller

In this section, we demonstrate the effects of uncertainty on the control trajectory of the HVAC system obtained using the proposed L-EMPC controller. We carry out the described experiment in Section IV-A, however, now also including uncertainty in the building thermal model. Note that dynamical model (3) and (4) for the building thermal load can be stated as follows:

$$\boldsymbol{x}^{k+1} = \boldsymbol{A}\boldsymbol{x}^k + \boldsymbol{B}\boldsymbol{u}^k \circ (\boldsymbol{T_s} - \boldsymbol{y}^k) + \boldsymbol{E}\boldsymbol{d}^k + \boldsymbol{E}\boldsymbol{\phi}^k \quad (38)$$

In (38), only the term $\boldsymbol{E}\boldsymbol{\phi}^k$ is unknown. Here, we assume $\boldsymbol{\phi}^k$ is chosen in a way that the entries of the term $\boldsymbol{E}\boldsymbol{\phi}^k$ have a uniform distribution which is represented as $unif(a, b)$ for any two real numbers $b > a$.

For both occupancy patterns, Fig. 7 shows the optimal air mass flow and the consequent evolution of indoor thermal zone temperature using the L-EMPC when controlling the HVAC system with a uncertainty of $unif(-2, 2)$ in the building thermal model. This leads to $\pm 2(^\circ C)$ uncertainty in system states i.e. room temperature. Then, these trajectories are compared with their corresponding nominal trajectories derived by the NL-EMPC without any model uncertainty.

As it can be seen in Fig.7a and Fig.7b, for the considered model uncertainty, the L-EMPC controller can control the

room temperature with an acceptable accuracy. Note that there are minor constraint violations due to the model uncertainty during a few time-intervals of the day (e.g. between 10:00 and 12:00 for the occupancy pattern 2). As it was described in Section III-B, due to the use of receding horizon control approach the controller includes the effects of the observed model uncertainty (at the current time-step) when optimizing for the future time-steps. The economical effects of the model uncertainty can be seen in Figs.7e and 7f, where power consumption pattern for the building load is lower and higher compared to the nominal power consumption trajectory for occupancy patterns 1 and 2, respectively. The deviation from nominal power trajectory is explained as follows. Due to the model uncertainty, the observed system states are different from predicted/assumed system states. Therefore, the controller adjusts the air mass flow rate by re-optimizing the problem for the current sampling time after including the effects of uncertainty on the system states that are observed at the current sampling time. Thus, the air mass flow and consequently power consumption of the HVAC system under the model uncertainty follow different trajectories compared to their nominal trajectories without any model uncertainty.

Note that, in the presence of uncertainty, the controllers are still able to ensure user comfort while optimizing for the economic objective. The errors in model estimation and errors in environmental disturbance prediction contribute to the cumulative uncertainty in the dynamical model for the building thermal loads as discussed in Section III B. Advanced model estimation techniques [20] and prediction methods [37] can help reduce the cumulative uncertainty. Therefore, the proposed nominal EMPC models are used for controlling the building thermal load as they do not deteriorate the control decisions due to model uncertainty while providing significant computational advantages compared to the robust EMPC.

D. L-EMPC: Co-scheduling HVAC, PV and Battery Storage

This section demonstrates the effectiveness of the L-EMPC controller in meeting the economic objective of minimizing transacted energy cost by coordinating the HVAC system control with the battery energy storage, the PV system, and other inflexible loads of the building. We divide results to two different scenarios, namely, *Scenario*-I and *Scenario*-II. In *Scenario*-I, the depreciation cost of the battery is ignored ($Price_b = 0$) and similar to the Section IV-A, we compare the results against an equivalent NL-EMPC controller. In *Scenario*-II, we show the capability of the proposed controller for co-scheduling different sources of energy and buildings' load with a more complicated model for the battery in which depreciation cost of the battery is considered. For both *Scenario*-I and *Scenario*-II, the building thermal dynamical model simultaneously utilizes the occupancy information and TOU prices to optimally schedule all resources. The PV panel is rated at 4 kW. The actual PV generation follows the sun's irradiation during the day, and it is depicted in Fig. 8a. It is assumed that the battery is in the minimum state of charge ($SOC = 0.25$) at the beginning of the one-day simulation (00:00). Fig.8b shows the demand profile for other essential

This article has been accepted for publication in a future issue of this journal, but has not been fully edited. Content may change prior to final publication. Citation information: DOI 10.1109/TSG.2020.2965559, IEEE Transactions on Smart Grid

12

(a) PV generation vs irradiation

(b) Power demand of inflexible load
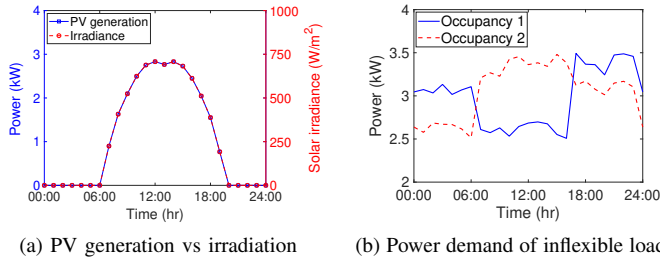
Fig. 8. Model Parameter for Co-Scheduling Energy

and inflexible building loads; the demand varies based on the building occupancy patterns.

1) Scenario-I: Fig. 9 shows the schedule of purchased power for the day to satisfy the power requirement of a building's HVAC system and inflexible loads for both occupancy patterns and both NL-EMPC and L-EMPC controllers. Three scenarios are demonstrated: (1) without the battery storage and the PV, (2) with the battery storage but without the PV, and (3) with both the battery storage and the PV. As it can be observed for both occupancy patterns, with the help of the PV, a reduction in total amount of purchased power from the grid is observed. This reduction reaches its maximum at around 12:00 noon when there is maximum solar radiation. Similarly, the positive effect of the battery can be observed; the HEMS decides to purchase the energy at times that TOU electricity tariffs are low (00:00- 07:00) to charge the battery, and uses the stored energy when TOU electricity tariffs are high (17:00-21:00).

Next, Table II shows the cost of purchased electricity for each combination of resources to be co-scheduled. As it can be observed from this Table, the L-EMPC controller closely approximates the behavior of the NL-EMPC controller and effectively co-schedules all resources. The cost of pucharsed electricity for the day is approximately the same for both NL-EMPC and L-EMPC controllers. Therefore, the proposed L-EMPC controller can be used in place of the NL-EMPC without compromising the performance while significantly improving the computational efficiency. Notice that on co-scheduling the HVAC system with the battery, the cost of electricity usage is decreased for the day. As expected, co-scheduling the HVAC system with both PV and battery storage leads to the most savings in electricity usage cost.

TABLE II
TOTAL COST OF ELECTRICITY USAGE DURING A DAY (24-HOURS)

Approach	Occupancy Pattern	Cost Based on System Configurations($)		
		Loads	Loads+Battery	Loads+Battery+PV
NL-EMPC	Occupancy pattern 1	3.3287	3.2594	1.8521
	Occupancy pattern 2	3.9115	3.8053	2.3979
L-EMPC	Occupancy pattern 1	3.3287	3.2545	1.8471
	Occupancy pattern 2	3.9137	3.7929	2.3856

2) Scenario-II: As it was mentioned in Section III, considering the depreciation cost of the battery introduces binary variables in the problem formulation. This changes the formulation for the L-EMPC controller to the MIL-EMPC (mixed-integer linear EMPC) controller. Therefore, the aforementioned solvers in Table I cannot be used in this section and new solvers are required to solve the mixed-integer linear programming problem associated with MIL-EMPC model.

We use CPLEX to solve the MIL-EMPC formulation. Here, we consider different depreciation costs for the battery and evaluate the role of this parameter in co-scheduling HVAC system, PV, and battery storage.

Fig.10 shows the purchased power during the day for the aforementioned test scenarios based on the MIL-EMPC formulation for four separate battery depreciation cost parameters. The cases with no depreciation cost for the battery i.e. $Price_b = 0$ \$/MWh and for $Price_b = 15$ \$/MWh, result in the same optimal power consumption trajectory (see Fig. 9). In fact, as long as the depreciation cost of the battery is lower than the minimum predicted TOU electricity tariffs for the day, regardless of the depreciation cost, the controller schedules the battery in a way to get the most possible economic benefit. Therefore, the building loads have the same power consumption pattern for all depreciation costs less than the minimum predicted TOU electricity tariffs. When the depreciation cost of the battery lies between the minimum and the maximum predicted TOU electricity tariffs (e.g. $Price_b = 40$\$/MWh), economical benefits that can be obtained from charging/discharging of the battery are reduced as the controller limits the battery operation based on the relative TOU electricity tariffs and the battery depreciation cost. For example, the oscillations due to charging and discharging of the battery in the case of with $Price_b = 15$\$/MWh cannot be seen in some time intervals of the case with $Price_b = 40$ (e.g. from 22:00 to 23:00 for the occupancy pattern 2), as discharging the battery in the latter case is not economically beneficial. Finally, for the case that depreciation cost of the battery is more than the maximum predicted TOU electricity tariffs (e.g. $Price_b = 75$\$/MWh), controller prevents the battery from discharging for all the times which is equivalent to the case of having no battery storage in the building.

Table III shows the cost of purchased electricity for different cases simulated for battery depreciation costs for the two defined occupancy patterns. For both occupancy patterns, as it was expected for $Price_b = 15$ \$/MWh, when the battery

(a) NL-EMPC (occupancy 1)

(b) NL-EMPC (occupancy 2)

(c) L-EMPC (occupancy 1)

(d) L-EMPC (occupancy 2)
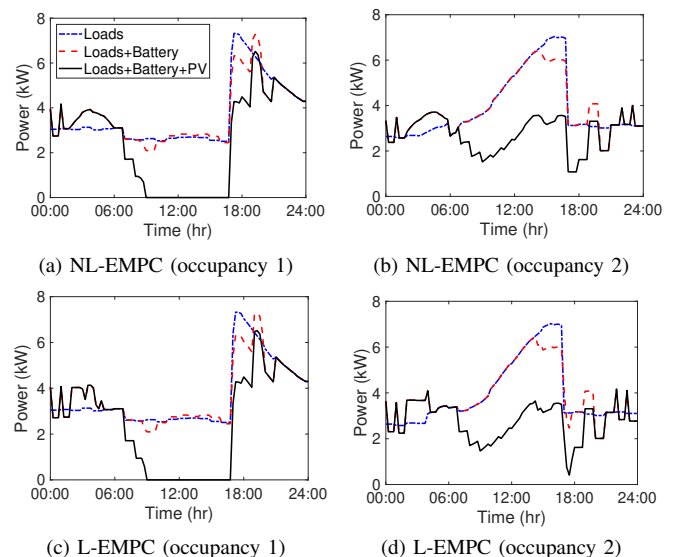
Fig. 9. Amount of purchased power during a day under different system configurations for EMPC controllers and defined occupancy patterns.

(a) occupancy pattern 1   (b) occupancy pattern 2
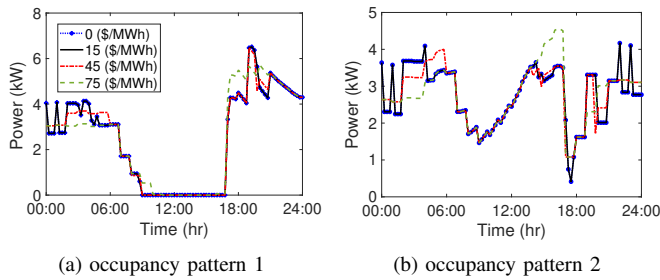
Fig. 10. Amount of purchased power during a day based on different depreciation costs of the battery for MIL-EMPC controllers and defined occupancy patterns.

depreciation cost is lower than the minimum forecasted TOU price, the total cost of purchased electricity is the minimum. These minimum values can vary up to \$1.9584 and \$2.5063 for the occupancy pattern 1 and the occupancy pattern 2, respectively; where due to the higher depreciation cost of the battery compared to the TOU electricity tariffs rendering the battery operation is uneconomical and its charging/discharging is restricted.

TABLE III
TOTAL COST OF ELECTRICITY USAGE DURING A DAY (24-HOURS)

Occupancy Pattern	Depreciation Cost of a Battery(\$)			
	0(\$MWh)	15(\$MWh)	40(\$MWh)	75(\$MWh)
Occupancy pattern 1	1.8471	1.8471	1.8577	1.9584
Occupancy pattern 2	2.3856	2.3856	2.4364	2.5063

V. CONCLUSION

In this paper, we developed a novel L-EMPC controller that can mimic the behavior of the NL-EMPC controller for building HVAC systems. In order to approximate the nonlinear dynamics of the system, several methods were proposed including feedback linearization for nonlinear control input, constraint mapping based-on prediction, and function approximation using piecewise linearization. The proposed L-EMPC controller can successfully optimize the buildings' electricity usage cost by leveraging the known buildings' occupancy information, a dynamical model of the HVAC system, and projected DER generation. The results obtained using the proposed L-EMPC controller were thoroughly bench-marked against the NL-EMPC controller. Specifically, for a price-sensitive control of building's HVAC system, we demonstrated that for a negligible value of error, the L-EMPC controller can dramatically improve the computation time. Then, we showed that the L-EMPC controller can precisely co-schedule building's HVAC system with its inflexible loads, the PV system, and the battery storage.

APPENDIX A
MIXED-INTEGER LINEAR FORMULATION FOR THE BATTERY STORAGE SYSTEM

The constraint (11) can be re-written as follows:

$$P_d^k = \begin{cases} |P_{c,d}^k| & \text{if } -P_{c,d}^k > 0 \\ 0 & \text{otherwise} \end{cases} \qquad (39)$$

We use a binary variable and Big-M method [38] to model different conditions of (39). First, we define a binary variable to activate different boundaries of (39). This can be stated as follows:

$$\delta = 1 \Longleftrightarrow -P_{c,d}^k > 0 \qquad (40)$$
$$\delta = 0 \Longleftrightarrow -P_{c,d}^k \leqslant 0$$

This can be formulated as:

$$-P_{c,d}^k \geqslant \epsilon - M(1 - \delta) \qquad (41)$$
$$-P_{c,d}^k \leqslant M\delta \qquad (42)$$

where $\delta \in \{0, 1\}$, ϵ and M are binary variable, arbitrary small number and arbitrary large number, respectively, which are used to model (40). It should be noted that M should be chosen as a big enough (possibly always different) number so that it does not limit any significant function of variables in the constraints [38]. Also, ϵ is used to guarantee that for $\delta = 1$, $P_{c,d}^k$ is not equal to zero. Then, we model conditions of (39) based on (40) as follows:

$$\delta = 1 \Longleftrightarrow P_d^k = |P_{c,d}^k| \qquad (43)$$
$$\delta = 0 \Longleftrightarrow P_d^k = 0$$

This can be formulated as:

$$|P_{c,d}^k| - M(1 - \delta) \leqslant P_d^k \leqslant |P_{c,d}^k| + M(1 - \delta) \qquad (44)$$
$$-M\delta \leqslant P_d^k \leqslant M\delta \qquad (45)$$

where the double inequality (44) still needs to be linearized due to the absolute value term. Thus, the left hand-side inequality of (44) can be re-written as follows:

$$|P_{c,d}^k| \leqslant P_d^k + M(1 - \delta) \qquad (46)$$

which can be linearized as follows:

$$P_{c,d}^k \leqslant P_d^k + M(1 - \delta) \qquad (47)$$
$$-P_{c,d}^k \leqslant P_d^k + M(1 - \delta) \qquad (48)$$

Then, the right hand-side inequality of (44) can be stated as follows:

$$|P_{c,d}^k| \geqslant P_d^k - M(1 - \delta) \qquad (49)$$

which can be linearized as follows:

$$P_{c,d}^k \geqslant P_d^k - M(1 - \delta) - M\beta \qquad (50)$$
$$-P_{c,d}^k \geqslant P_d^k - M(1 - \delta) - M(1 - \beta) \qquad (51)$$

where $\beta \in \{0, 1\}$ is a binary variable which is defined to linearize (49). Therefore, the nonlinear constraint (11) can be replaced by set of mixed-integer constraints (41), (42), (45), (47), (48), (50) and (51). Interested readers are encouraged to refer [33] and [38] for more details.

REFERENCES

[1] M. Pazhoohesh and C. Zhang, "Investigating occupancy-driven air-conditioning control based on thermal comfort level," *Journal of Architectural Engineering*, vol. 24, no. 2, p. 04018003, 2018.
[2] Y. Liu, N. Yu, W. Wang, X. Guan, Z. Xu, B. Dong, and T. Liu, "Coordinating the operations of smart buildings in smart grids," *Applied Energy*, vol. 228, pp. 2510–2525, 2018.
[3] M. Ostadijafari, A. Dubey, Y. Liu, J. Shi, and N. Yu, "Smart building energy management using nonlinear economic model predictive control," *arXiv preprint arXiv:1906.00362*, 2019.
[4] Y. Long, S. Liu, L. Xie, and K. H. Johansson, "A hierarchical distributed mpc for HVAC systems," in *American Control Conference (ACC), 2016.* IEEE, 2016, pp. 2385–2390.
[5] J. Cigler, "Model predictive control for buildings," 2013.
[6] M. Maasoumy and A. Sangiovanni-Vincentelli, "Total and peak energy consumption minimization of building HVAC systems using model predictive control," *IEEE Design & Test of Computers*, vol. 29, no. 4, pp. 26–35, 2012.

This article has been accepted for publication in a future issue of this journal, but has not been fully edited. Content may change prior to final publication. Citation information: DOI 10.1109/TSG.2020.2965559, IEEE Transactions on Smart Grid

14

[7] G. Mantovani and L. Ferrarini, "Temperature control of a commercial building with model predictive control techniques," *IEEE Transactions on Industrial Electronics*, vol. 62, no. 4, pp. 2651–2660, 2015.

[8] J. Rehrl and M. Horn, "Temperature control for HVAC systems based on exact linearization and model predictive control," in *Control Applications (CCA), 2011 IEEE International Conference on*. IEEE, 2011, pp. 1119–1124.

[9] T. Wei, Q. Zhu, and M. Maasoumy, "Co-scheduling of HVAC control, ev charging and battery usage for building energy efficiency," in *Proceedings of the 2014 IEEE/ACM International Conference on Computer-Aided Design*. IEEE Press, 2014, pp. 191–196.

[10] T. Wei, Q. Zhu, and N. Yu, "Proactive demand participation of smart buildings in smart grid," *IEEE Transactions on Computers*, vol. 65, no. 5, pp. 1392–1406, 2016.

[11] M. Ostadijafari and A. Dubey, "Linear model-predictive controller (lmpc) for building's heating ventilation and air conditioning (hvac) system," in *2019 IEEE Conference on Control Technology and Applications (CCTA)*, Aug 2019, pp. 617–623.

[12] Y. Ma, F. Borrelli, B. Hencey, B. Coffey, S. Bengea, and P. Haves, "Model predictive control for the operation of building cooling systems," *IEEE Transactions on control systems technology*, vol. 20, no. 3, pp. 796–803, 2012.

[13] J. Cigler, D. Gyalistras, J. Široky, V. Tiet, and L. Ferkl, "Beyond theory: the challenge of implementing model predictive control in buildings," in *Proceedings of 11th Rehva world congress, Clima*, vol. 250, 2013.

[14] A. Mirakhorli and B. Dong, "Model predictive control for building loads connected with a residential distribution grid," *Applied energy*, vol. 230, pp. 627–642, 2018.

[15] A. F. Taha, N. Gatsis, B. Dong, A. Pipri, and Z. Li, "Buildings-to-grid integration framework," *IEEE Transactions on Smart Grid*, 2017.

[16] A. Vosughi, M. Xue, and S. Roy, "Occupant-location-catered control of iot-enabled building hvac systems," *IEEE Transactions on Control Systems Technology*, pp. 1–9, 2019.

[17] M. M. Haghighi and A. L. Sangiovanni-Vincentelli, "Modeling and optimal control algorithm design for HVAC systems in energy efficient buildings," *Masters report*, 2011.

[18] A. Bemporad and M. Morari, "Robust model predictive control: A survey," in *Robustness in identification and control*. Springer, 1999, pp. 207–226.

[19] G. Serale, M. Fiorentini, A. Capozzoli, D. Bernardini, and A. Bemporad, "Model predictive control (mpc) for enhancing building and hvac system energy efficiency: Problem formulation, applications and opportunities," *Energies*, vol. 11, no. 3, p. 631, 2018.

[20] M. Maasoumy, M. Razmara, M. Shahbakhti, and A. S. Vincentelli, "Handling model uncertainty in model predictive control for energy efficient buildings," *Energy and Buildings*, vol. 77, pp. 377–392, 2014.

[21] S. Privara, J. Cigler, Z. Váňa, F. Oldewurtel, C. Sagerschnig, and E. Žáčeková, "Building modeling as a crucial part for building predictive control," *Energy and Buildings*, vol. 56, pp. 8–22, 2013.

[22] M. J. Siemann, "Performance and applications of residential building energy grey-box models," Ph.D. dissertation, 2013.

[23] D. Sturzenegger, D. Gyalistras, M. Gwerder, C. Sagerschnig, M. Morari, and R. S. Smith, "Model predictive control of a swiss office building," in *Clima-rheva world congress*, 2013, pp. 3227–3236.

[24] S. Prívara, Z. Váňa, D. Gyalistras, J. Cigler, C. Sagerschnig, M. Morari, and L. Ferkl, "Modeling and identification of a large multi-zone office building," in *2011 IEEE International Conference on Control Applications (CCA)*. IEEE, 2011, pp. 55–60.

[25] H. Shareef, M. S. Ahmed, A. Mohamed, and E. Al Hassan, "Review on home energy management system considering demand responses, smart technologies, and intelligent controllers," *IEEE Access*, vol. 6, pp. 24 498–24 509, 2018.

[26] M. Beaudin and H. Zareipour, "Home energy management systems: A review of modelling and complexity," *Renewable and sustainable energy reviews*, vol. 45, pp. 318–335, 2015.

[27] J. Cai, X. Jin, and H. Zhang, "Economic model-based control of sustainable buildings with photovoltaic (PV) and battery systems considering battery degradation costs," in *2018 Annual American Control Conference (ACC)*. IEEE, 2018, pp. 5406–5411.

[28] P. Zhou, W. Dai, and T.-Y. Chai, "Multivariable disturbance observer based advanced feedback control design and its application to a grinding circuit," *IEEE Transactions on Control Systems Technology*, vol. 22, no. 4, pp. 1474–1485, 2014.

[29] H. K. Khalil and J. Grizzle, "Nonlinear systems, vol. 3," *Prentice hall Upper Saddle River*, 2002.

[30] M. A. Henson and D. E. Seborg, "Feedback linearizing control," *Nonlinear process control*, vol. 149, 1997.

[31] M. J. Kurtz and M. A. Henson, "Input-output linearizing control of constrained nonlinear processes," *Journal of Process Control*, vol. 7, no. 1, pp. 3–18, 1997.

[32] A. Ghasemi, "Application of linear model predictive control and input-output linearization to constrained control of 3d cable robots," *Modern Mechanical Engineering*, vol. 1, no. 02, p. 69, 2011.

[33] M. Bernreuther, "Solving mixed-integer programming problems using piecewise linearization methods," 2017.

[34] A. Marquez, J. Patino, and J. Espinosa, "Min-max economic model predictive control," in *53rd IEEE Conference on Decision and Control*. IEEE, 2014, pp. 4410–4415.

[35] F. A. Bayer, M. A. Müller, and F. Allgöwer, "Tube-based robust economic model predictive control," *Journal of Process Control*, vol. 24, no. 8, pp. 1237–1246, 2014.

[36] S. Subramanian, S. Lucia, and S. Engell, "Economic multi-stage output nonlinear model predictive control," in *2014 IEEE Conference on Control Applications (CCA)*. IEEE, 2014, pp. 1837–1842.

[37] https://scijinks.gov/forecast-reliability.

[38] M. S. Bazaraa, J. J. Jarvis, and H. D. Sherali, *Linear programming and network flows*. John Wiley & Sons, 2011.

Mohammad Ostadijafari (S'18) received the B.S. and M.S. degree in Electrical Engineering from Islamic Azad University at Tehran, Iran, in 2013 and 2015, respectively. He is currently working toward the Ph.D. degree at the School of Electrical Engineering and Computer Science, Washington State University, Pullman, WA, USA. His current research interests include energy management in smart buildings, power market and application of the control theory in power systems.

Anamika Dubey (M'16) received the M.S.E and Ph.D. degrees in electrical and computer engineering from the University of Texas at Austin, Austin, TX, USA, in 2012 and 2015, respectively. She is currently an Assistant Professor with the School of Electrical Engineering and Computer Science, Washington State University (WSU), Pullman, WA, USA. Her research focus is on the analysis, operation, and planning of the modern power distribution systems for enhanced service quality and grid resilience. At WSU, her lab focuses on developing new planning and operational tools for the current and future power distribution systems that help in effective integration of distributed energy resources and responsive loads.

Nanpeng Yu (M'11-SM'16) received his B.S. in Electrical Engineering from Tsinghua University, Beijing, China, in 2006. Dr. Yu also received his M.S. and Ph.D. degree in Electrical Engineering from Iowa State University, Ames, IA, USA in 2007 and 2010 respectively. He is currently an Associate Professor in the department of Electrical and Computer Engineering at University of California, Riverside, CA, USA. His current research interests include machine learning theory, big data analytics in smart grid, electricity market design, and smart energy communities. Dr. Yu is an Editor of IEEE Transactions on Smart Grid, IEEE Transactions on Sustainable Energy, and International Transactions on Electrical Energy Systems.